Supporting Information

A Silk Fibroin Cryogel Building Adaptive Organohydrogels with Switching Mechanics and Viscoelasticity

Berkant Yetiskin, and Oguz Okay *

Department of Chemistry, Istanbul Technical University, Maslak, 34469 Istanbul, Turkey.
E-mail: okayo@itu.edu.tr

Table of Contents

Cyclic strain-sweep tests on SF cryogel

The cyclic compression shown in Fig. 2b reveals reversible flow-out and flow-in of water through the pores of the cryogel under high and low strain, respectively. This means that, if the strain is applied to a cryogel specimen confined between the parallel plates of a rheometer, the flow-out water will surround the specimen providing its liquid-like response to the stress whereas upon reducing the applied strain, flow-in water will recover its gel-like response. We recently demonstrated this behavior in hyaluronic acid cryogels.[S1] In order to verify this interesting phenomenon for the present cryogels, we conducted cyclic strain-sweep tests on a cryogel specimen between 1 and 100% strains (γ_0) at a fixed frequency ω of 6.3 rad s^{-1}. Figure S5 shows γ_0-dependent variations of *G'* (filled symbols), *G''* (open symbols), and *tan* δ (lines) of a cryogel specimen formed at 5 w/v % SF and 2 w/v % DMAA. Results of up and down strain sweep tests are shown by circles and triangles, respectively. It is seen that *G''* starts to dominate over *G'*, i.e., an apparent gel-to-sol transition takes place at ~15% strain above which the cryogel behaves as a low density liquid. The cryogel regain its initial viscoelastic properties after reducing the strain back to 1%, revealing the reversibility of the solid to liquid-like transition. It is worth to mention that this gel-to-sol transition is only an apparent transition because the cryogel network remains intact under strain while the rheometer measures the response of the flowing-out water surrounding the gel. This behavior thus verifies the cyclic compressibility of SF cryogels.

[S1] Tavsanli, B.; Okay, O. Macroporous Hyaluronic Acid Cryogels of High Mechanical Strength and Flow-Dependent Viscoelasticity. *Carbohydr. Polym.* **2020**, 229, 115458.

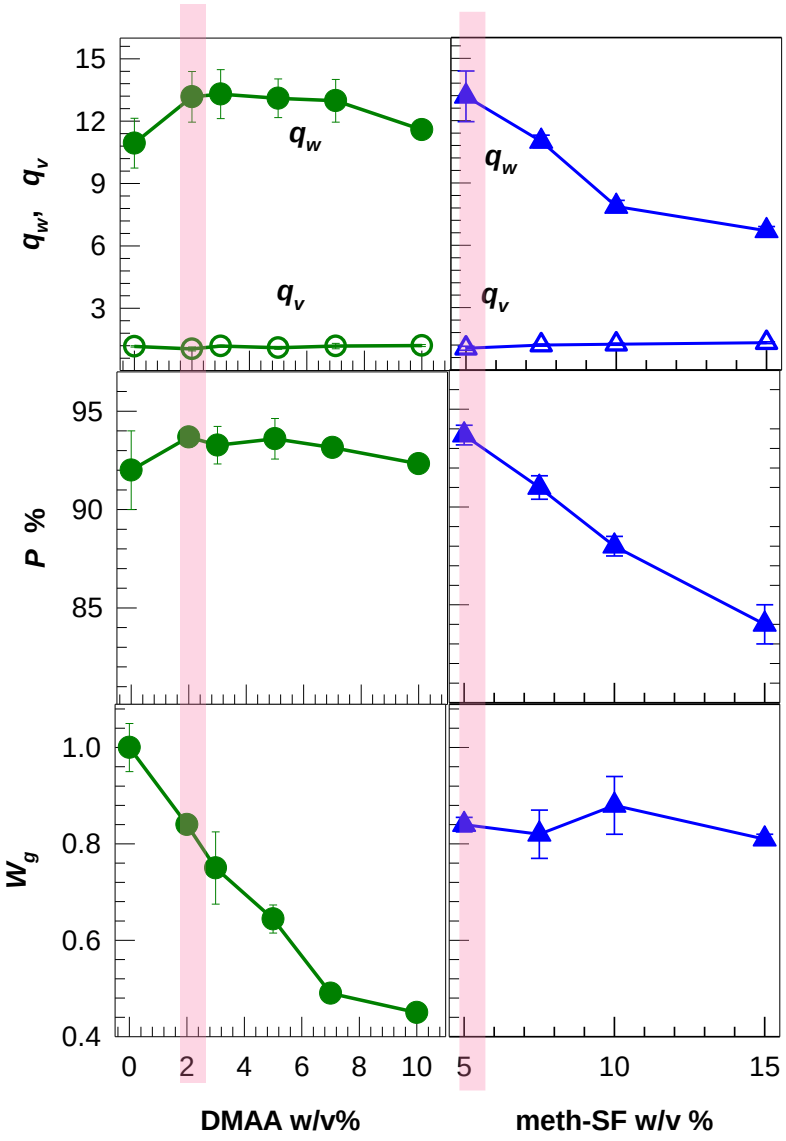

Figure S1. The weight (q_w) and volume swelling ratios (q_v) in water, the total porosity P, and the gel fraction W_g of the cryogels. They were prepared at 5 w/v% meth-SF and at various DMAA w/v % (left panel), and at 2 w/v% DMAA and at various meth-SF w/v % (right panel). The colored bars represent the cryogel selected for OHG preparation.

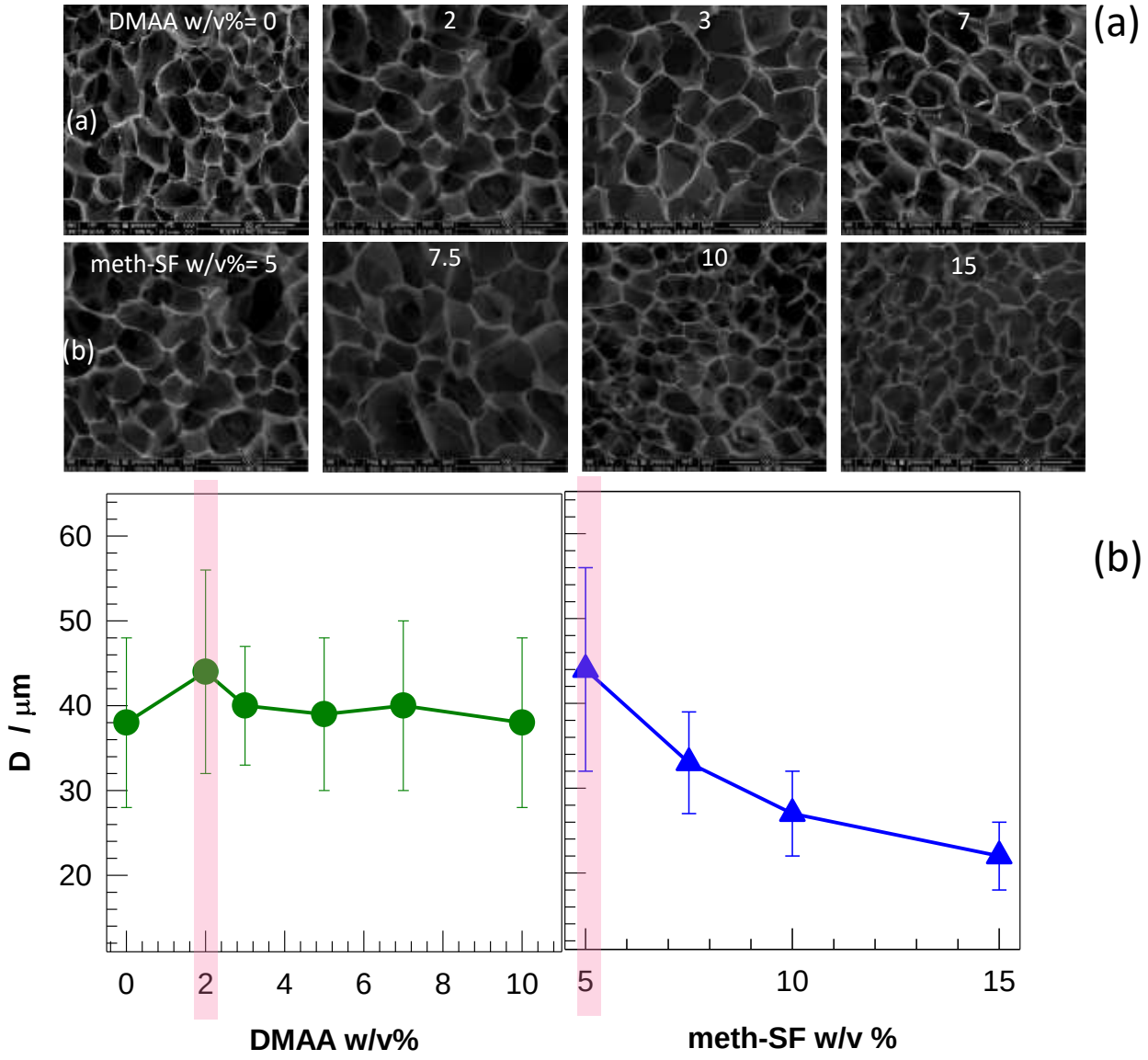

Figure S2. (a) SEM images of the cryogel scaffolds formed at 5 w/v% meth-SF and at various DMAA w/v % (upper panel), and at 2 w/v% DMAA and at various meth-SF w/v % (bottom panel). (b) The average pore diameter *D* of the cryogel scaffolds plotted against the DMAA and meth-SF concentrations. The colored bars represent the cryogel selected for OHG preparation.

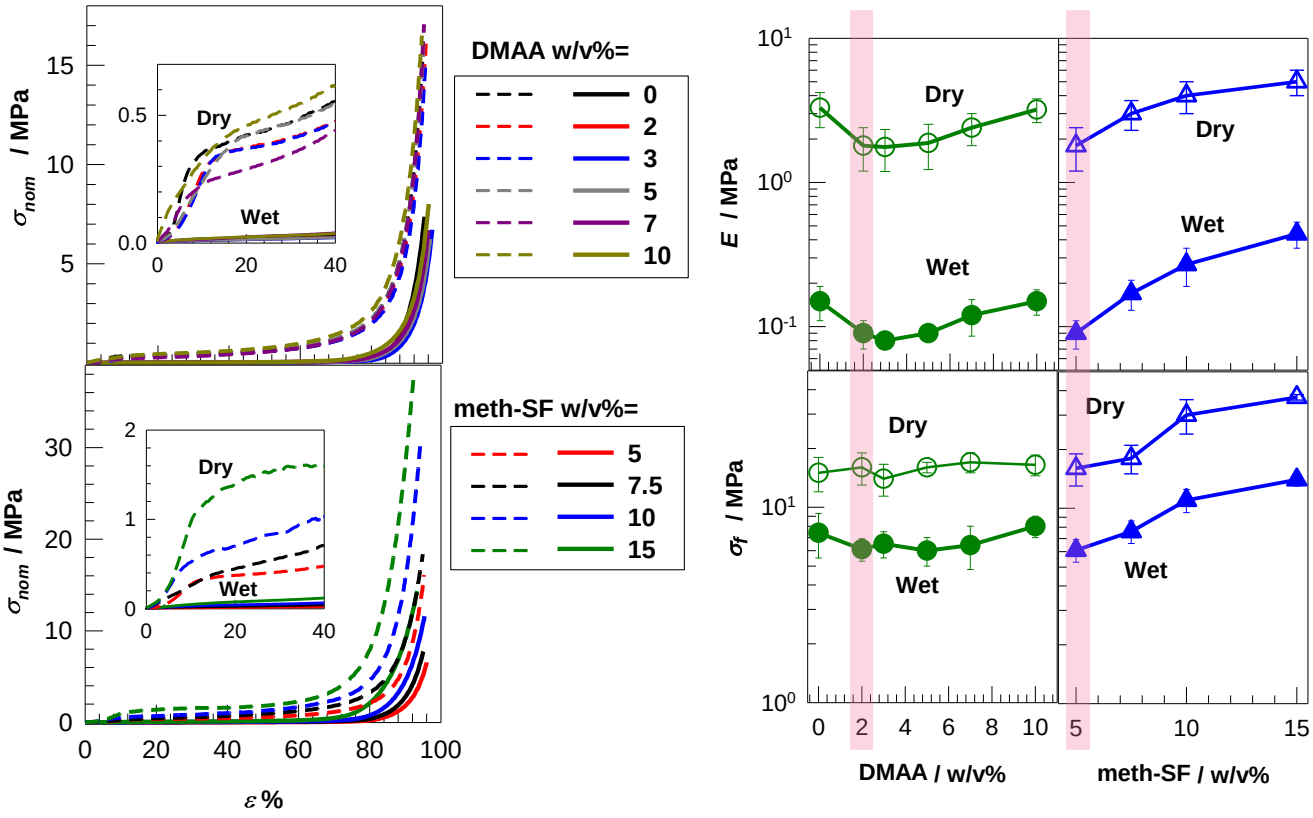

Figure S3. The compressive stress – strain curves of the cryogels in wet (solid curves) and dry states (dashed curves), and their mechanical parameters. The cryogels were prepared at 5 w/v% meth-SF and at various DMAA w/v %, and at 2 w/v% DMAA and at various meth-SF w/v %. The colored bars represent the cryogel selected for OHG preparation.

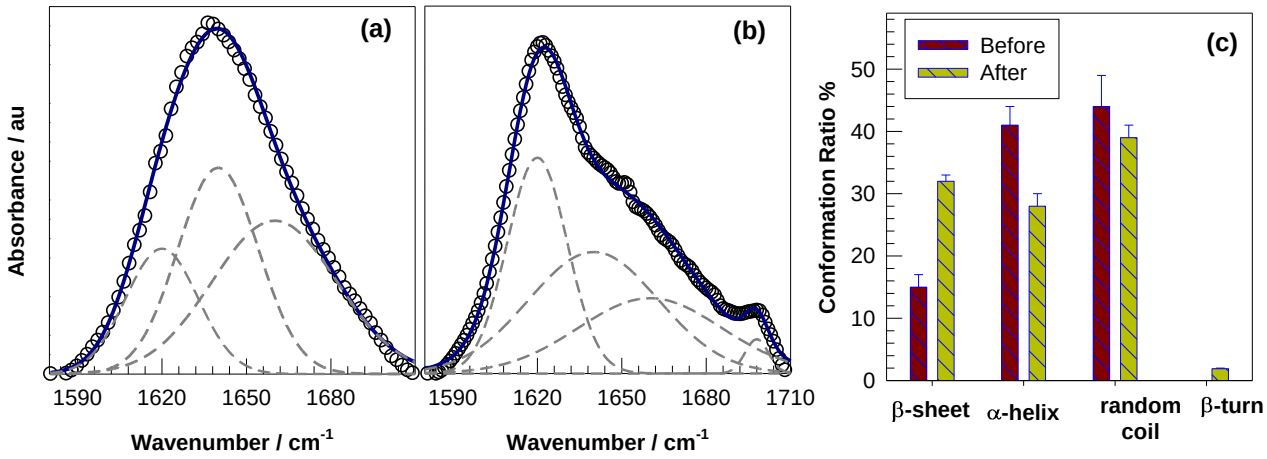

Figure S4. (a,b) Amide-I region of the FTIR spectra of meth-SF before (a) and after cryogelation (b). The symbols are the original data while the solid and dashed curves represent the fitted spectra and hidden peaks, respectively. The bands at 1620, 1640, 1660 and 1698 cm^{-1} correspond to β-sheet, random coil, α-helix and β-turn respectively. (c) The conformation ratios of meth-SF before and after cryogelation.

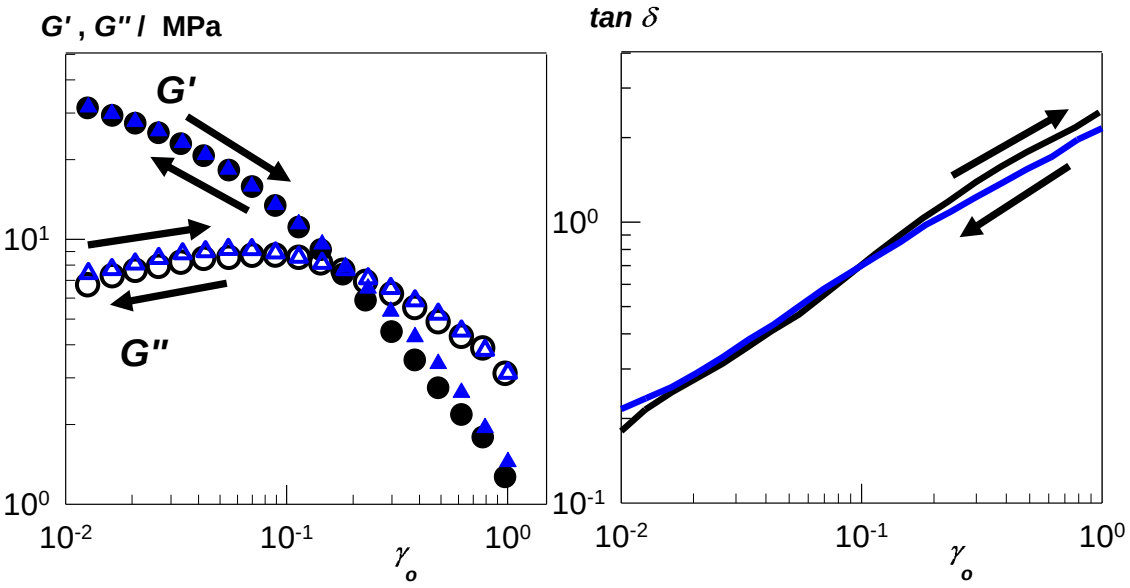

Figure S5. *G'* (filled symbols), *G''* (open symbols), and loss factor *tan δ* of a cryogel specimen formed at 5 w/v % SF and 2 w/v % DMAA as a function of strain γ_o. ω = 6.3 rad·s^{-1}. Dynamic moduli data of up and down strain sweep tests are shown by the circles and triangles, while *tan δ* data are shown by the black and blue lines, respectively. Temperature = 25 °C.

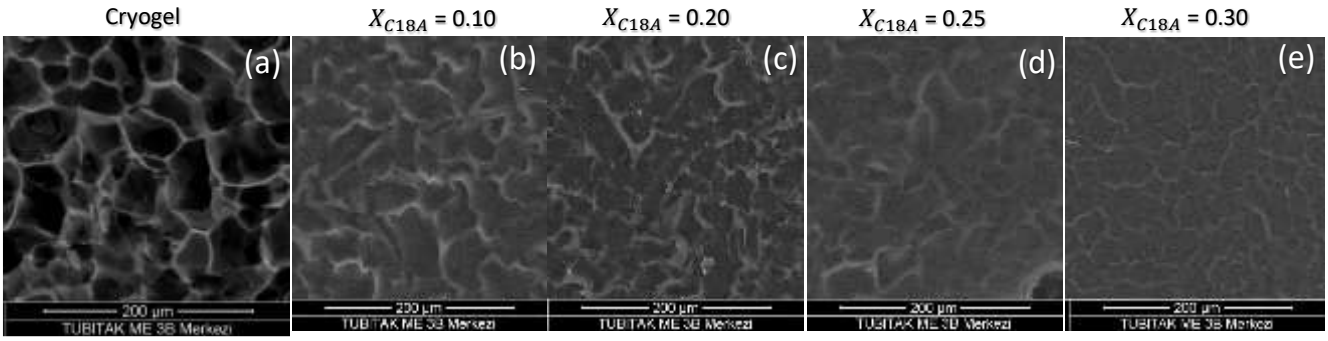

Figure S6. SEM images of the cryogel (a), and OHGs prepared at various x_{C18A} as indicated (b-e). Scale bars = 200 µm.

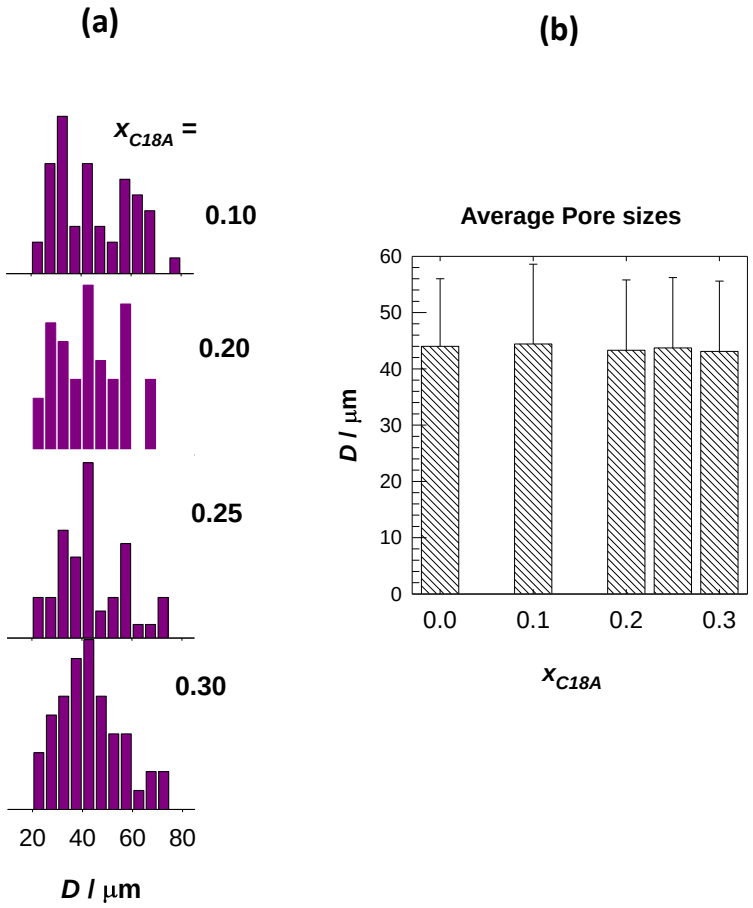

Figure S7. The pore size distribution (a) and the average pore diameter *D* (b) of OHGs formed at various x_{C18A}. The size distribution and the average diameter of the pores were estimated by analyzing at least 50 pores in the SEM images taken at various magnifications.

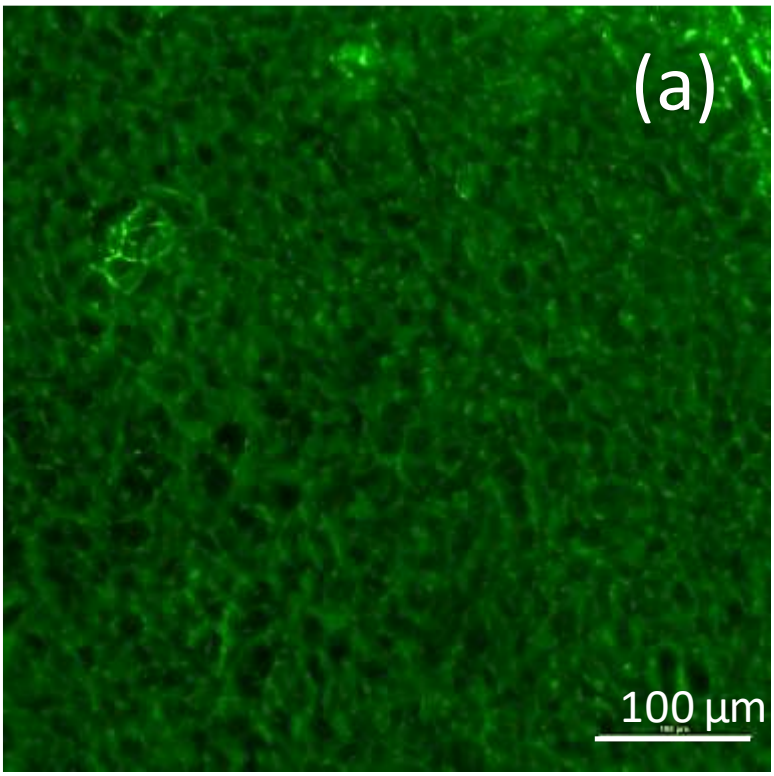
(a)
100 µm

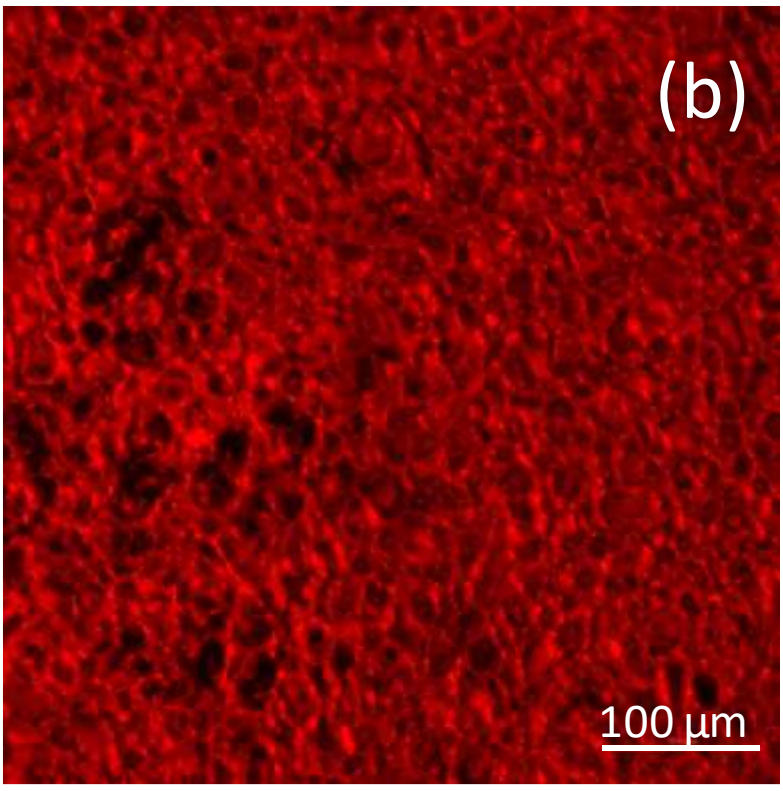
(b)
100 µm

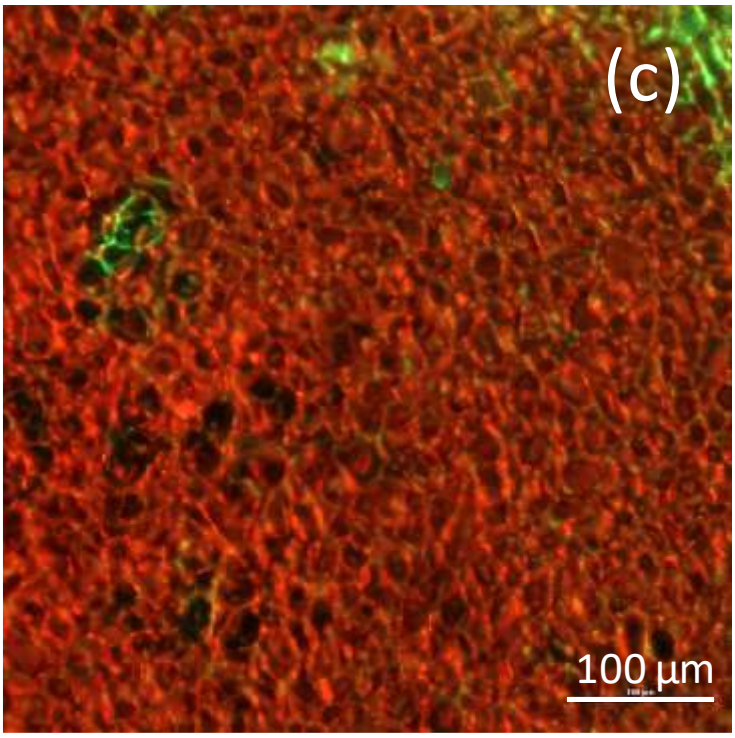

Figure S8. Confocal microscopy images of the OHG formed at x_{C18A} = 0.30. The cryogel scaffold was stained green using FITC while poly(AAc-co-C18A) micro-inclusion was stained with nile red. The images show the SF scaffold (a) and organogel phases (b), and the OHG (c).

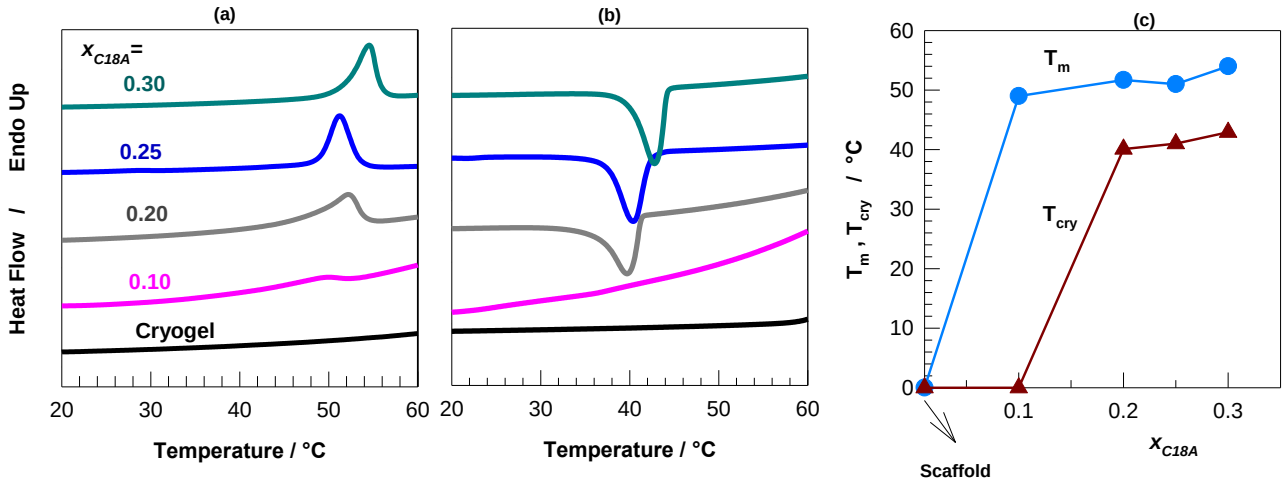

Figure S9. (a, b) DSC scans of OHGs during heating (a) and cooling (b). (c) The melting T_m and crystallization temperatures T_{cry} of OHGs plotted against x_{C18A}.

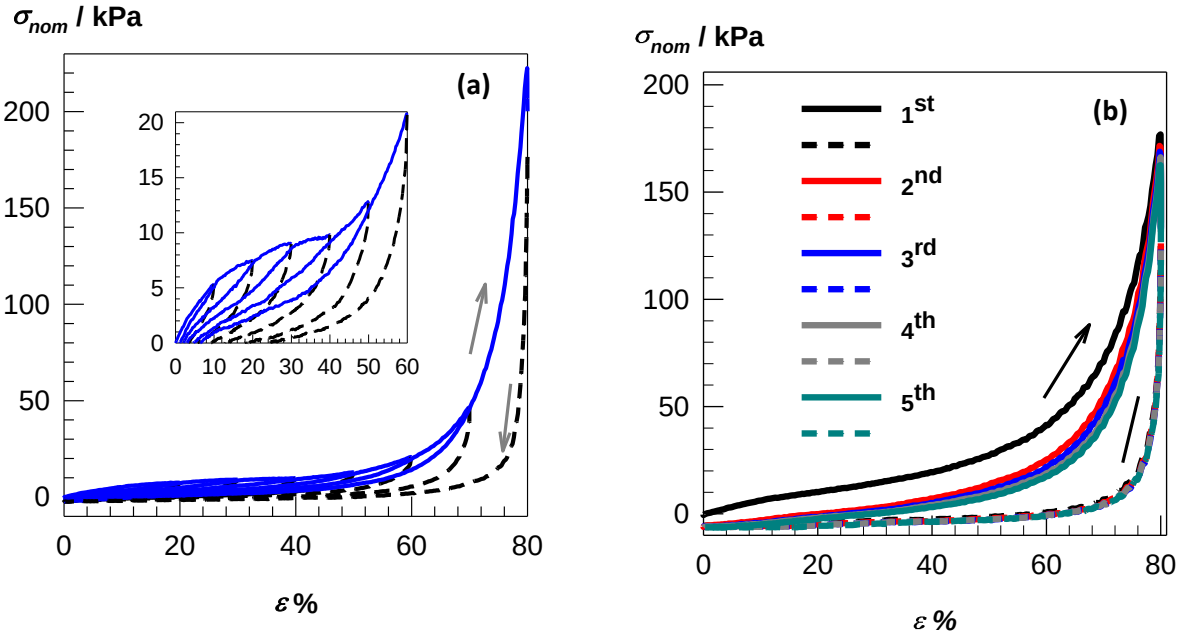

Figure S10. Successive loading and unloading cycles of a cryogel specimen formed at 5 w/v % meth-SF and 2 w/v % DMAA. (a) Eight successive cycles with increasing ε_{max} from 10 to 80%. (b) Five successive cycles up to a fixed ε_{max} of 80%. Loading and unloading curves are shown by the solid and dashed curves, respectively.